Performance improvement in a supercontinuum fiber-coupled system for near infrared absorption spectroscopy

SILJE SKEIDE FUGLERUD,[1,2,*] JONG WOOK NOH,[1] ASTRID AKSNES,[1] AND DAG ROAR HJELME [1]

[1]*Department of Electronic Systems, Norwegian University of Science and Technology, Trondheim, Norway*
[2]*Department of Endocrinology, St. Olavs University Hospital, Trondheim, Norway*
[*]*silje.fuglerud@ntnu.no*

Abstract: High fidelity near infrared spectroscopy (NIRS) requires high signal to noise ratio (SNR) achieved with costly and often bulky components in benchtop setups. Portable spectrometers are available but lack the accuracy to measure analytes in small quantities in, for example, aqueous samples. Towards high accuracy portable NIRS, we present a fully fiber optic spectroscopy setup with a supercontinuum source in the long-pulse regime (2 ns). The noise sources of the system are studied theoretically and experimentally. The relative intensity noise (RIN) was reduced from typical values up to 6 % to less than 0.1 % by deploying a balanced detector and averaging. At well-balanced wavelengths, the system without transmission cells achieved an SNR above 70 dB, approaching the shot noise limit. With transmission cells and long-term measurements, the overall SNR was 55 dB. Glucose in physiological concentrations was measured as a model system, yielding a root mean square error of 4.8 mM, approaching the needed accuracy for physiological glucose monitoring.

1. Introduction

Quantitative near infrared spectroscopy (NIRS) for measurement of low concentrations of trace components in fluids requires careful configurations and optimization of the instrumentation, including calibration and system stability [1]. Therefore, such applications normally require the use of expensive benchtop systems limiting applications of NIRS outside controlled environments. One way to bring higher accuracy NIRS to field applications could be to use optical fiber-coupled broad bandwidth sources with high spectral power density and compact and rugged spectrometers [2] in a fully optical fiber-coupled system. Optical fibers in the near infrared (NIR) range come at a low cost due to their use in telecommunications, and can improve the robustness of a setup by replacing bulk optics and simplifying packaging and assembly.

Spatially coherent broad bandwidth sources with high spectral power density are now readily available. Robust and relatively inexpensive supercontinuum (SC) sources are replacing more traditional light sources in a number of applications, like optical coherence tomography (OCT) [3–5] and stimulated Raman scattering (SRS) microscopy [6,7]. Within NIRS, special applications like ultra-high repetition rate absorption spectroscopy have been successful [8–10]. However, utilizing the broad spectrum from SC sources in conventional NIR absorption spectroscopy is challenging due to the high relative intensity noise (RIN) [4, 11]. A low-noise SC source was only recently demonstrated [5] and might be expected to come at a higher cost if reaching commercialization in the near future. Close to shot noise limited detection using commercially available high RIN SC sources might be possible using a balanced detection scheme, i.e. by using a reference arm for an independent measurement of the source noise. However, in practice the difficulty to maintain precise balance of the two arms limits the achievable noise suppression. In the area of Raman spectroscopy, various balancing schemes to account for variations in the

sensing arm relative to the reference arm have been developed [7, 12, 13]. This is made possible by the non-linear interaction and the pump-probe configuration of the systems. Unfortunately, these methods are not readily available for linear absorption spectroscopy set-ups. The achievable performance of fully fiber-coupled NIR absorption based sensor systems using SC sources remains unknown.

Implementing balanced detection schemes over a broad spectral range for optical fiber coupled NIR absorption spectroscopy systems is challenging for a number of reasons including: i) wavelength dependent splitting ratio of beam splitters and couplers, ii) modal interference, or modal noise, in multi mode (MM) optical fiber systems, and iii) path length difference in the reference and sensing absorption cell in cases when the solvent (background medium) has wavelength dependent absorption. The last point is particularly challenging for NIR absorption measurements in aqueous samples. Modal noise of MM fused couplers is an issue if the wavelength resolution required is lower than a few tens of nanometers [14, 15]. MM systems therefore usually rely on bulk optics with low insertion loss to avoid modal noise limitations. Any coupling noise in the absorption cells will also result in modal noise [16–18].

In this work, we will show how a NIRS system based on an SC source, balanced detection and fiber optics can be designed and optimized to meet the required accuracy for many field applications. To our knowledge, this is the first study exploring the various design considerations outlined above for a fully fiber-coupled NIR absorption spectroscopy based sensor system utilizing an SC source. We systematically characterize the noise sources and how they can be reduced.

To quantify the results of design choices, we have performed a case study using a commercial SC source for fiber-coupled NIR absorption spectroscopy in the wavelength range from 1400 nm to 1700 nm, to sense physiological concentrations of aqueous glucose. Combining bright SC sources and fiber optics can be a possible solution towards measuring glucose by NIR spectroscopy in vivo. Despite 40 years of research on non-invasive glucose sensing using NIRS and a trail of startups, a device capable of commercialization has not been obtained, partly due to the low glucose signal hidden within confounding factors [19], and difficulties translating the calibration across patients and different conditions [20]. A solution might be to apply NIRS to measure in a body fluid, such as peritoneal fluid, which is less influenced by confounding factors [21, 22]. Benchtop spectrometer solutions have obtained the required accuracy [23], but are not useful for in vivo measurements.

2. Theoretical background

2.1. Noise sources and formalism

The noise variance in a laser-system can be defined as

$$\sigma_{\text{tot}}^2 = \sigma_{\text{r+d}}^2 + \sigma_{\text{tec}}^2 + \sigma_{\text{shot}}^2 + \sigma_{\text{ex}}^2. \tag{1}$$

The first and second term, the receiver and detector noise $\sigma_{\text{r+d}}^2$ and technical noise σ_{tec}^2, are independent of the laser power. In publications describing similar applications [4, 5], Eq. 1 is defined without the term σ_{tec}^2. The receiver and detector noise, $\sigma_{\text{r+d}}$, is caused by the electronics in the photodetector and receiver, and quantization error in digitization. The technical noise, σ_{tec}, is caused by slow changes within the system due to temperature and mechanical instabilities and drift. The third term, σ_{shot}^2, represents the shot noise, and is linearly related to the incoming optical power [24, Ch. 12.2], $\sigma_{\text{shot}}^2 \propto S$, where S is the quantity that corresponds to the light intensity (e.g. measured counts, power, voltage). The shot noise is a fundamental physical limit and can only be reduced by limiting the measurement bandwidth. The fourth term, σ_{ex}^2, is the excess laser noise, which reflects the source relative intensity noise. The RIN is the normalized σ_{ex} expressed by $\sigma_{\text{ex}}/\bar{S}$, where $\bar{S}$ is the average of S. The excess laser noise variance is squarely proportional to the power [4]. The magnitude of the RIN is related to the source in use, and is

known to be a large contributor in SC sources. To highlight the dependence on source power, we express the system noise as

$$\sigma_{\text{tot}}^2 = a_0 + a_1 S + a_2 S^2, \tag{2}$$

where a_0, a_1, a_2 are coefficients determined by the instrumentation and S is the measured quantity related to the light intensity. The actual observed noise variance depends on the integration time and the number of samples averaged. If the power spectral density is flat, the variance scales linearly with bandwidth. Similarly, if N samples are integrated, the variance scales with $1/N$ [24]. The total relative noise can be expressed as the coefficient of variation (CV = $\sigma_{\text{tot}}/\bar{S}$).

The constant noise term a_0 encompasses all source power independent contributions, including the readout noise and technical noise sources such as modal noise, mechanical instability and quantization noise. Modal noise in MM fibers is caused by small perturbations of the fiber combined with spatial aperturing of the mode-dependent speckle pattern [17,18]. External factors such as temperature, mechanical movement of the fiber, or air flow conditions can influence the relative phase between excited modes [15]. Using single mode (SM) fibers eliminates modal noise, but with a disadvantage of higher coupling losses due to a smaller core and numerical aperture. The effect of modal noise was investigated experimentally for different conditions by Oliva et al. [25], and the signal to noise ratio (SNR) was decreased approximately 10 dB when a mechanical disturbance to the fiber was introduced but depended on the illumination conditions. By applying a mechanical agitator (fiber shaker), the SNR could be improved 5 dB due to averaging across the phase differences between the modes, yet this is not a viable solution for all applications.

To utilize absorption spectroscopy sample interaction must take place, in which the light passes through some sort of transmission cell for aqueous samples. Another noise source adding to the constant noise term can be caused by physical misalignment if the parts to the transmission cell are not completely fixed. In a glued holder, mechanical strain in the system can cause small movement of the fibers leading to a change in transmission. For example, if the path length changes with 1 µm, the water absorption will change by 0.04 ‰ (see S1A, Supplement 1).

The quantization error of digitizing a signal can be approximated to $1/2^n$ [26], where n is the number of bits. When measuring a small absorber with a large variation in background such as water, the quantization error is applied to the full water absorption, and the small absorption signal "riding" on this large signal can be lost in the quantization. Using a balanced detector will decrease the background considerably, allowing an order of magnitude higher difference signal gain. By introducing a balanced detector and increasing the signal gain by 10 dB or more, the bit resolution requirement can be reduced. A higher bit resolution increases the analog-to-digital converter (ADC) cost considerably and also constrains the bandwidth resolution.

2.2. Beer Lamberts law using a balanced detector

Beer-Lambert's law states that there is a linear relation between the absorbance A at a given wavelength and the concentration c of n absorbing analytes in a sample. It can be formulated as

$$A \equiv -\ln\left(\frac{I}{I_0}\right) = \sum_{i=1}^{n} \alpha_i l = \sum_{i=1}^{n} \epsilon_i c_i l, \tag{3}$$

where I and I_0 are the signal intensity and the reference intensity, α_i is the absorption coefficient for the given analyte, ϵ_i is the molar absorptivity, and l is the path length. A balanced detector consists of two inputs with balanced optical paths for sample and reference and outputs a voltage linearly related to the optical power in the two arms, $U_{\text{bal}} = (P_{\text{samp}} - P_{\text{ref}})\Re G$, where $\Re, G$ are the responsivity and transimpedance gain for the detector, respectively. The balanced scheme enables low-noise detection of an analyte with orders of magnitude lower absorption coefficient than the solvent, such as glucose. For an ideal balanced detector, the resulting difference signal

for an analyte in water becomes (see Supplement 1 S1D for the full calculation for glucose):

$$U_{\text{bal,analyte}} = \left(\epsilon_{H_2O} f c_A - \epsilon_A c_A\right) l U_{\text{unbal}} \tag{4}$$

for small (mM) concentrations. Here, f is the displacement factor for the reduction in water concentration by the analyte (glucose: [27]). U_{unbal} is the signal measured with optical power only in the reference arm (with water in the transmission cell) and can therefore be written as $U_{\text{unbal}} = \exp\left(-\alpha_{H_2O} l\right) I_0 A_{\text{det}} \Re G/2$, A_{det} is the illuminated area on the detector and a 50:50 split is assumed. Thus, the analyte concentration is directly proportional and linear in relation to the measured difference signal, given that the terms stay constant.

2.3. Shot noise estimation

The shot noise limit is a useful estimate to obtain a lower bound on the achievable stability. An estimate of the coefficient of variation ($\text{CV} = \sigma_{\text{tot}}/\bar{S}$) originating from the shot noise is

$$\text{CV}_{\text{shot}} = \sqrt{\frac{4eMGB}{NU_{\text{unbal}}}}, \tag{5}$$

where B is the bandwidth, G is the transimpedance gain of the detector, M is the number of sample points acquired per pulse, and N is the number of pulses averaged (details in S1D in Supplement 1). The shot noise limit for a balanced detector is 3 dB higher than the shot noise for a single detector [28] since the balance is the difference between two separate detectors. The gain factor is given as 1×10^3 V/A [29] for the balanced detector in use, but was also estimated to 0.4×10^3 V/A from the optical power and voltage response, which shows that the estimate is somewhat uncertain. We keep the gain estimate at $G = 1 \times 10^3$ V/A to set an upper bound for the shot noise. The estimates assume dependent samples, due to the oversampling of the detector.

2.4. Reduction in RIN in balanced detector

The common mode rejection ratio (CMRR) of a balanced detector reflects how much of the common noise can be removed. The output signal expressed as a function of CMRR reads [30]

$$U_{\text{bal}} = G(P_{\text{samp}} - P_{\text{ref}}) + \frac{G}{\text{CMRR}} \frac{1}{2} (P_{\text{samp}} + P_{\text{ref}}). \tag{6}$$

We can express $P_{\text{samp}} + P_{\text{ref}} = P_0$ and $P_{\text{samp,ref}} = C_{\text{samp,ref}} P_0$ representing the splitting ratios. The ratio between the balanced and unbalanced signal (with power in the sample arm and reference arm blocked) can then be described as

$$\frac{U_{\text{bal}}}{U_{\text{unbal}}} = 2(C_{\text{samp}} - C_{\text{ref}}) + \frac{1}{\text{CMRR}}, \tag{7}$$

where we have assumed that the CMRR is large and that the split ratio is close to 1/2. For CMRR= 30 dB [29] and perfect split ($C_{\text{samp}} = C_{\text{ref}}$), only 3 % of the original RIN remains ($\sigma_{\text{bal,50:50}} = 0.03\sigma_{\text{unbal}}$). For the case to be presented later, some wavelengths have a poorer balance with $C_{\text{samp}} = 0.44, C_{\text{ref}} = 0.56$. With such a balance, the remaining RIN is 31 % ($\sigma_{\text{bal,44:56}} = 0.31\sigma_{\text{unbal}}$). Thus, obtaining a good balance on the full broadband spectrum is important to achieve low noise levels on all wavelengths.

2.5. Case study: Stability requirements for glucose measurements

As previously reported in [11], the low absorption coefficient of glucose in the NIR range requires high SNR of a system measuring glucose at physiological levels. Within the first overtone band (1500 nm to 1850 nm) that is the focus of this work, the glucose absorption coefficient is

$\alpha_g < 1 \times 10^{-4}\,\mathrm{mM^{-1}mm^{-1}}$. The water absorption coefficient in the same wavelength region is $\alpha_w > 0.2\,\mathrm{mm^{-1}}$. The molar absorptivities for water and glucose from [27] are shown graphically in Figure 1(a). Water dominates as a solvent because the concentration is > 1000× higher than the glucose concentration. In the first overtone band, a change in glucose concentration of 1 mM is a change of less than on average 7.5×10^{-3} % (electrical SNR ~ 82 dB) of the full unbalanced signal, as shown in Figure 1(b). The noise levels should be lower than the signal ($\sigma_0/\bar{S} < 7.5 \times 10^{-3}$ %). The electrical SNR of the photoelectric current or voltage S_{el} is defined as [24, Ch. 18.6]

$$\mathrm{SNR} = \frac{\bar{S_{\mathrm{el}}}^2}{\sigma^2} \quad \text{or} \tag{8}$$

$$\mathrm{SNR_{dB}} = 20 \log \left(\frac{\bar{S_{\mathrm{el}}}}{\sigma} \right). \tag{9}$$

The accuracy required at each wavelength can be relaxed because the measurements are a scan across wavelengths (and time) that can result in correlated measurements. Trend analysis can therefore be utilized. By using dimensionality reduction, a set of spectra for different concentrations can be reduced to N_v orthogonal vectors (latent variables) comprised of p wavelengths [31]. Since the wavelengths p are correlated, a crude estimate of an increase in the accepted variance is p/N_v. The standard deviation should then be lower than $\sigma_{\mathrm{meas}} < \sigma_0\sqrt{p/N_v}$. We require a coefficient of variation (CV) less than 0.03 % (SNR ~ 70 dB) applying a number of 60 wavelengths and $N_v = 3$ which is realistic for the measurement setup to be presented, i.e. giving a 12 dB reduction.

Other wavelength regions of interest are the combination band and short-wave infrared (SWIR) band. The SWIR (900 nm to 1450 nm) has been investigated for non-invasive glucose measurements due to favorable tissue light absorption in this wavelength range (therapeutic window), and absorption from glucose has been shown between 1000 nm to 1400 nm [32, 33], but without stating molar absorptivities of glucose for the range. Studies investigating the most informative NIR wavelengths for glucose spectroscopy emphasize the first overtone and combination band [34, 35]. The combination band (2050 nm to 2300 nm) has a higher absorption cross section, but will not be included here due to instrumental limitations. This would require use of a photodetector with orders of magnitude higher dark currents [36, 37].

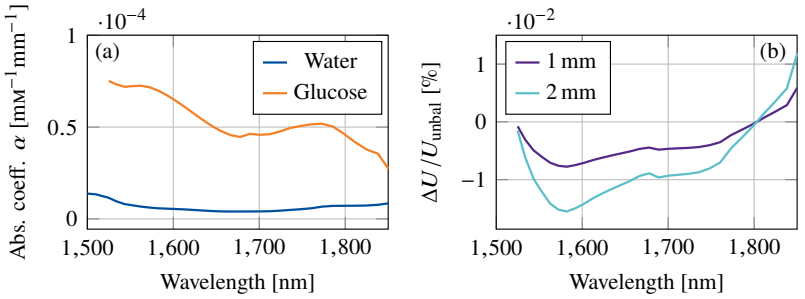

Fig. 1. (a) From literature [27]: The molar absorptivity of water and glucose at 37 °C. The concentration of pure water is more than 1000× higher than physiological glucose levels. (b) The estimated difference in the signal of the balanced detector for a 1 mM change in glucose concentration for path lengths l = 1 and 2 mm from Eq. 4 with data in (a) as input.

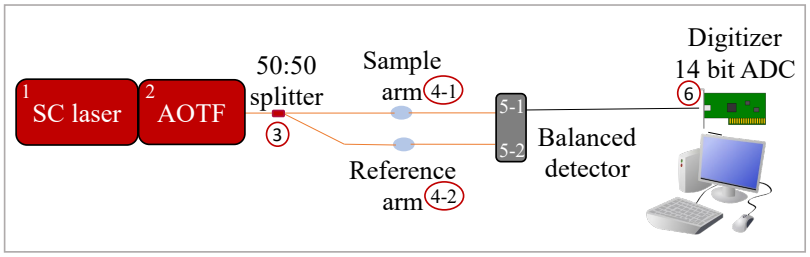

Fig. 2. Schematic of the experimental setup. The components are labeled for easier reference throughout the text.

3. Experimental section

3.1. Methods

Figure 2 shows the system setup, consisting of a Q-switched pumped SuperK Compact SC laser (1) with approximately 2 ns pulse length set to 18.4 kHz repetition rate, paired with an acousto-optic tunable filter (AOTF) (2) with wavelength selection in the NIR range covering 1175 nm to 2000 nm and with a spectral bandwidth of 6.4 nm to 19.8 nm. The AOTF can also regulate the laser power amplitude in increments of 1 % of the original power, which is tabulated to 200 mW across the full spectral range. Using the AOTF (set to 100 % transmitted laser power amplitude), we measured 0.09 mW output power for $\lambda = 1315$ nm, with a corresponding linewidth of > 6.4 nm. Four 50:50 splitters (3) were investigated: a MM fused splitter, a SM fused splitter, a MM mirror splitter, and a SM mirror splitter.

Two transmission cells (4-1,4-2) were manufactured by gluing two connector ends into bronze sleeves with a machined window that ensured alignment with 2 mm path length (details in S2A, Supplement 1). The splitter and the transmission cells were connected with MM fibers for the MM splitters, and SM fibers for the SM splitters. 1 m long MM fibers were used to collect the light from the transmission cells and were coupled directly to the balanced detector (5).

The signals were received by a balanced detector (5) set to 150 MHz bandwidth and 1×10^3 V/A transimpedance gain. The wavelength range investigated (1175 nm to 1700 nm) was based on the AOTF limitation on the lower bound and the detector responsivity on the upper bound. The signal was digitized using a 500 MS/s 14 bit ADC digitizer card (6) set to measure with 125 MHz bandwidth to match the difference channel from the detector. The combination of the detector and digitizer was based on a holistic evaluation of cost and optimal bandwidth. The optimal SNR of a 2 ns pulse has been estimated to 50 MHz to 100 MHz [38]. The ADC card was connected directly to the pulse trigger from the laser with a BNC cable, and 10 sample points were integrated and recorded from every pulse, as shown in Figure 3.

A set of characterization experiments was performed to determine the optimal scanning parameters and to characterize the system, outlined in Table 1. The details about the measurement procedures can be found in Figure 3 and in Section S2A in Supplement 1. U_{unbal} refers to the measurement with one input blocked into the balanced detector (only measure 5-1 or 5-2). The first measurements characterized the system without the transmission cell (component 4).

The case study consisting of two glucose experiments was conducted afterwards (further details in Section S2A, Supplement 1):

1. Discrete measurements of glucose solutions in phosphate buffered saline (PBS) buffer in sample arm and PBS buffer in reference arm.

2. Continuous measurements of glucose solutions in PBS buffer (sample arm, PBS buffer in reference arm) pumped in steps as a function of time.

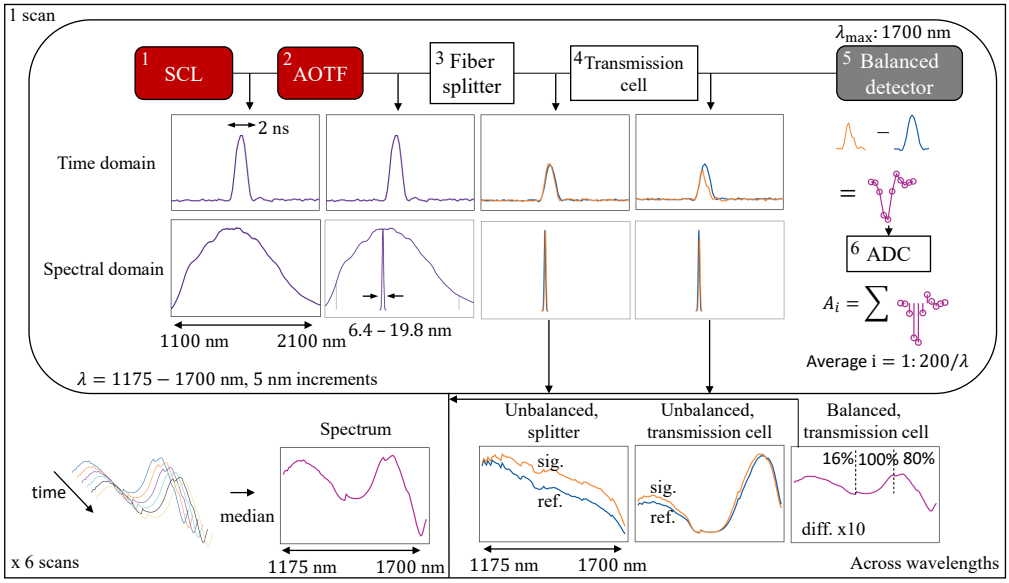

Fig. 3. Acquisition and signal processing. A narrow wavelength range was selected from pulses generated by the SC laser by the AOTF. The pulse was split in two by a fiber splitter and passed through two transmission cells. The pulses were received by a balanced detector and the difference signal was sampled by an ADC card. One value per pulse was obtained by integrating across ten measurement points. One spectral scan was obtained by averaging across 200 pulses, and iterating across 1175 nm to 1700 nm. A final spectrum was generated from the median across six scans to reduce the effect of outliers. On the bottom line, the unbalanced traces after the splitter and transmission cell with water are shown (power adjusted to avoid detector saturation) along with a balanced trace. Details and equipment numbers are shown in Table S4 (Supplement 1).

Component	Purpose	Measurement type	# pulses, (# scans)	Results
3. Optical fiber splitters	Critical component, select the most stable	RMS	200avg x 3	Fig. 4
1. System w/o balance w/o transmission cell	Quantify laser RIN	Std	1000	Fig. 5
5. System w/balanced detector w/o transmission cell	Quantify stability improvement,	Std	1000	Fig. 5
	optimize averaging,	Std	700 000	Fig. 6
	quantify CV w/avg,	Std	200avg x 11	Fig. 6
	long-term stability	Allan variance	200avg x 70, 209, 211	Fig. 9
1.,4.,5. System w/balance and transmission cells w/water	Quantify variance full system,	Std	1000	Fig. 7
	including averaging,	Std	200avg x 11	Fig. 7
	estimate noise contributions	Var vs mean	1000	Fig. 8

Table 1. Overview of characterization and measurements. Number of scans is mentioned when average across pulses were employed. If not, the standard deviation was computed across the pulses.

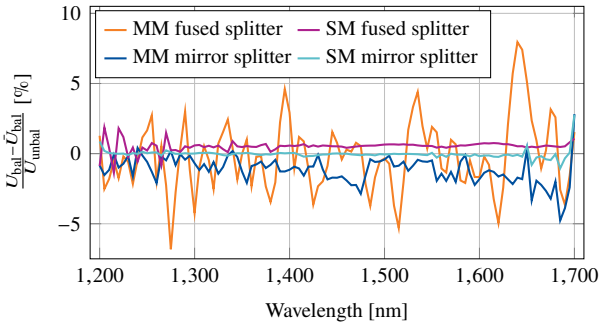

Fig. 4. Example of noise characteristics for the investigated fiber optic splitters (component 3). The optical fibers were moved between three scans obtained for each splitter. The traces show one of the scans, with the mean of the three scans with a three-point moving average subtracted for visibility.

The first experiment aimed at determining precision, whereas the second experiment mimics a physiological situation with fluid constantly changing, without the possibility to take blank samples. A blank spectrum of the buffer solution was subtracted from the discrete glucose measurement to account for experimental drift. For the time series, a blank spectrum of pure buffer was obtained in the beginning and at the end of the series, and a time dependent correction factor assuming linear drift was subtracted for each wavelength from the time series. Prediction models for the two experiments were built using partial least squares regression (PLSR) and cross-validation to obtain the optimal number of latent variables. These chemometric analysis techniques are standard in analysis of NIR spectra and provided in more detail elsewhere [31, 39].

3.2. Noise characterization

Effect of optical splitter and fiber components

The direct signal from the splitters was measured (averaged across 200 pulses) and the fibers going in and out of the splitters were moved between measurements (repeated three times). One of the traces obtained is shown in Figure 4 for all four splitters. The three-point moving mean average of the traces per splitter was subtracted for visibility. The mean rms across the spectra of the three traces in reference to a smoothed mean is shown in Table 2. The modal noise was a large noise contributor for the MM components. The output of the MM fused splitter was extremely unstable, and the difference signal changed with mechanical movements and temperature changes. Although the MM fused splitter transmitted seven times as much light as the other splitters, the instability and the sensitivity to mechanical movement are too high. The challenge using SC sources for this application is not low power (the source was attenuated to avoid detector saturation), but rather high noise levels.

	MM fused	MM mirror	SM fused	SM mirror
rms($\frac{U_{bal}-\bar{U}_{bal}}{U_{unbal}}$)	1.69 %	1.07 %	0.85 %	0.16 %

Table 2. Root mean square error difference from the mean from three traces where the optical fibers were moved between for each splitter, averaged across all wavelengths.

The fused splitters were also found to be more sensitive to changes in the room temperature and the air condition system flow rate setting than the mirror splitters in long-term experiments. The MM splitters have in common that the trace fluctuates across neighboring wavelengths, whereas

both the SM traces are smooth in comparison. The SM fused splitter can be seen to have a baseline shift, whereas the SM mirror splitter is the most stable splitter that was investigated. It is therefore used in the rest of the measurements and characterizations, along with SM illumination fibers between the splitter and transmission cells. An example of a balanced and unbalanced (reference intensity) trace are shown in the bottom line of Figure 3 for the SM mirror splitter coupled direcly to the detector, and through the transmission cell with water.

Noise suppression by balanced detector

The CV of the pure laser noise measured in one of the arms of the balanced detector was found to be from 2.8 % to 6 % across 1000 pulses as shown in Figure 5(a). This is the pulse-to-pulse variation that is dominated by the RIN and has been reported within similar levels for this laser type [3]. Note that this value is subject to spectral averaging due to the AOTF broadness (up to 19.8 nm), and a narrower filter would give a larger variance per wavelength [4]. With the only measure being the balanced detector, the CV was reduced to between 0.19 % and 1.5 %, a 24 dB reduction for 1550 nm. The measured balanced CV corresponds reasonably well with the predicted CV based on Eq. 7 with the split ratio in Figure 5(b) as input. The predicted CV for the balanced detector does not take the shot noise limit into account, which is a lower bound on the achievable CV.

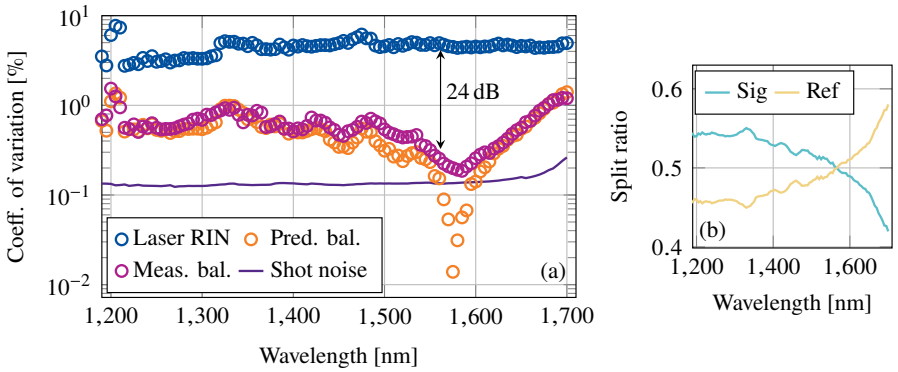

Fig. 5. (a) The measured laser RIN, the predicted standard deviation for the balanced case, the measured balanced standard deviation, and the predicted shot noise limit (Eq. 5). The predicted standard deviation was found using Eq. 7, based on measured split ratios shown in (b) and the measured laser RIN. The fibers were directly coupled from the SM mirror splitter and measured across 1000 pulses.

Noise reduction by averaging

If the noise in each sampled signal is uncorrelated, the SNR should increase by $\sqrt{N}$ across N averages. The effect of averaging was investigated across a measurement series including 700 000 consecutive pulses recorded per wavelength. The results are shown in Figure 6(a), for 1300 nm, 1500 nm and 1600 nm together with a guiding line indicating the $\sqrt{N}$ improvement. The well balanced wavelength 1600 nm deviates from the $\sqrt{N}$-line around 50 averages, whereas the less balanced 1300 nm starts out with a lower SNR and follows the $\sqrt{N}$-line almost up to 200 averages. The scan procedure was therefore set to 200 pulses per wavelength per scan. The difference between the measurement and ideal $\sqrt{N}$ line is smaller for 1300 nm than for the more balanced wavelengths because there is more random instability at 1300 nm, which can be improved by averaging. Low frequency noise and technical noise with long correlation times become more important on a longer time-scale.

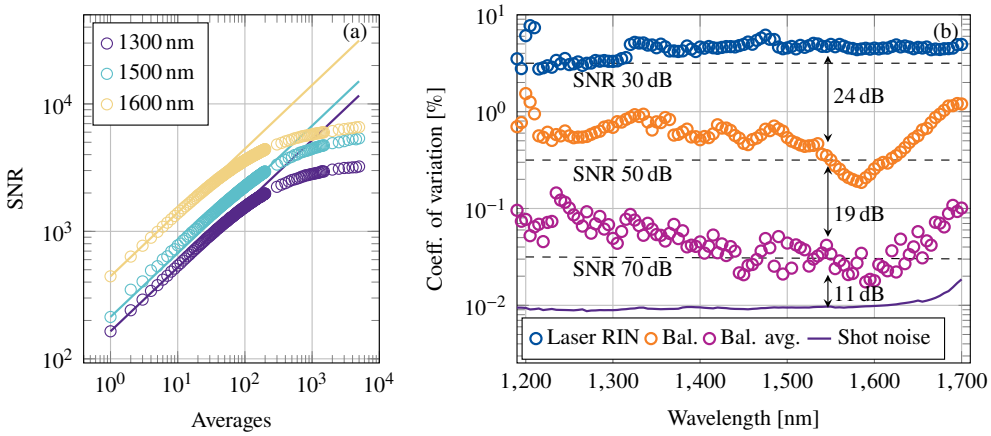

Fig. 6. (a) The improvement by averaging for different wavelengths compared to the $\sqrt{N}$ predicted improvement. (b) CV for the setup directly coupled from the split for the measured laser RIN, the measured CV with a balanced detector, the measured CV acquired with 200 averages, and the predicted shot noise limit (Eq. 5).

The total improvement from the original laser RIN-dominated standard variation in the directly coupled system can be seen in Figure 6(b) including averaging, with the measured CV between 0.018 % and 0.2 %. We obtained 19 dB lower noise at 1550 nm when averaging across 200 pulses, which matches well with a theoretical improvement of 23 dB corresponding to $1/\sqrt{200}$. The mean SNR with averaging was 66 dB.

Full system stability

With the introduction of the transmission cell, the CV increased to between 0.02 % and 1 %, as can be seen in Figure 7(a). Two 20 µL water drops were placed in the two transmission cells, and measured continuously. The high CV around 1400 nm is due to the high water absorption. The lower CV around 1650 nm can be attributed to a more favorable balance achieved with the water cells in combination with less water absorption than at other wavelengths. The splitting ratios for the transmission cells are shown in Figure 7(b). The split ratio for wavelengths between 1400 nm to 1420 nm is inaccurate due to almost zero transmission. The measured standard deviation deviates more from the estimated shot noise limit than the measurements without a water transmission cell. The short-term full system SNR was 58 dB, an 8 dB SNR reduction accompanied by the introduction of the transmission cells and the MM collection fibers compared to the stability for the directly coupled system shown in Figure 6.

Short-term noise contributions

The variance between consecutive measurements across 1000 pulses at one wavelength was recorded as a function of the input light level, which could be tuned by the AOTF. A polynomial fit was applied to the resulting relation in Figure 8 in order to determine the constant terms (in Eq. 2) for the shot noise and the excess laser noise. Within short time periods, the technical noise does not have a significant contribution, and it has therefore been omitted. The system is dominated by excess laser noise (not shot noise limited), but as the balance improves from 1550 nm to 1610 nm (see Figure 7(b)), the system variance approaches the shot noise limit. The SNR of the balanced pulses (no averaging) was up to 49 dB, which is 14 dB lower than that of the estimated shot noise limit from regression. For less balanced wavelengths, the difference was around 18 dB. The estimated shot noise from regression was a few dB higher than the predicted

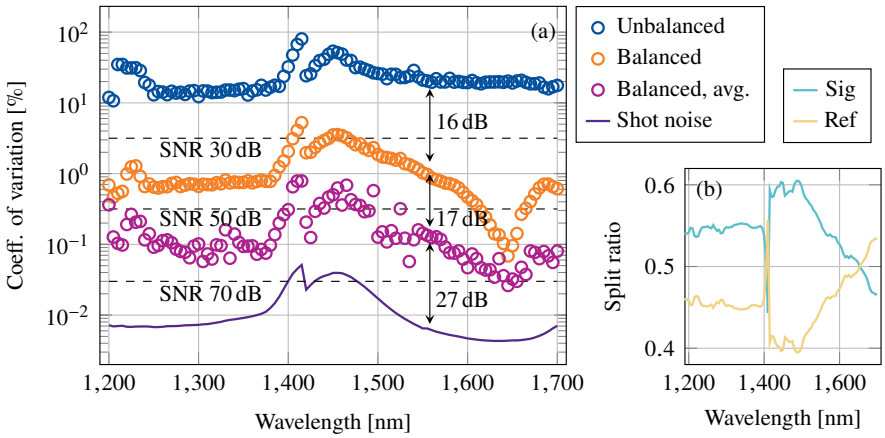

Fig. 7. (a) The CV for the system through the water cell, without balance showing added noise from the transmission cell in addition to the laser RIN, balanced, with 200 averages, and the predicted shot noise limit (Eq. 5). The discontinuity at 1420 nm is due to a change in the laser amplitude settings to avoid detector saturation. (b) The splitting ratios from the full setup with the water transmission cells.

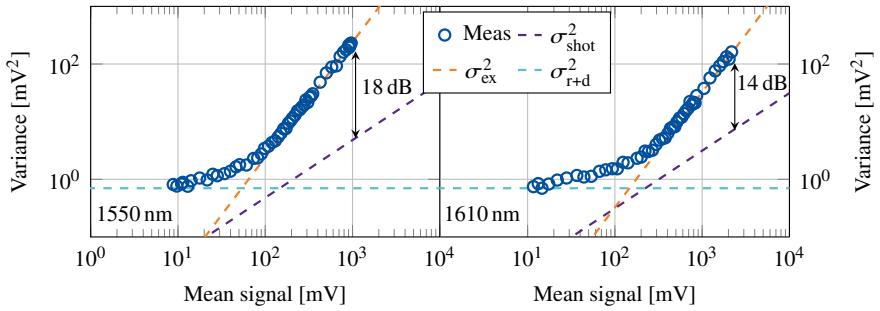

Fig. 8. The variance of the balanced signal through water as a function of the input light level at 1550 nm and 1610 nm with coefficients for the noise terms found by regression.

shot noise level from Eq. 5. The experimentally determined shot noise limit is perceived as more accurate, since the estimated limit is based on typical values for the gain and responsivity, which might differ in this exact setup.

Long-term stability

The long-term stability was investigated by Allan variance analysis. The SM mirror splitter was coupled directly to the balanced detector and scans were continuously recorded with 200 pulses per wavelength and 5 nm increments in three measurement series (one 74 min, two 230 min). The resulting average Allan variance across the three measurement series is shown in Figure 9(a) for four selected wavelengths. For all the wavelengths, there is an improvement in averaging across subsequent scans, and a high degree of stability up to approximately 15 min for most wavelengths. At longer time scales, the Allan variance increases at some wavelengths. The Allan variance for time constant $\tau = 32$ min is shown in Figure 9(b). The long-term stability declines for the wavelengths below 1400 nm and above 1600 nm. The splitter and fibers are optimized at 1550 nm,

and although the specified supported wavelengths span down to below 1300 nm, the balance is not as good at these wavelengths as around 1550 nm (see split ratio in Figure 5(b)). The slow change can be due to external factors such as temperature or mechanical changes affecting the splitter characteristics or laser characteristics which have more impact at wavelengths with less optimal balance. The changes in the temperature or laser characteristics over time could also affect polarization and guided modes in the system, which could give small changes in transmission in the splitter or aperture of the detector. On the basis of the poor long-term stability of the lower wavelengths and to reduce acquistion time, only wavelengths > 1400 nm were included in the following case study. We chose to record the higher wavelengths due to a better balance through the transmission cells (Figure 7(b)). Based on these and similar stability recordings for this system, we included 6 scans with a reduced scan measurement time (40 s) and created the spectrum by taking the median of the 6 consecutive scans on every wavelength. We obtained a more stable signal less influenced by outliers due to technical noise that was not suppressed by averaging consecutive pulses by taking the median instead of averaging.

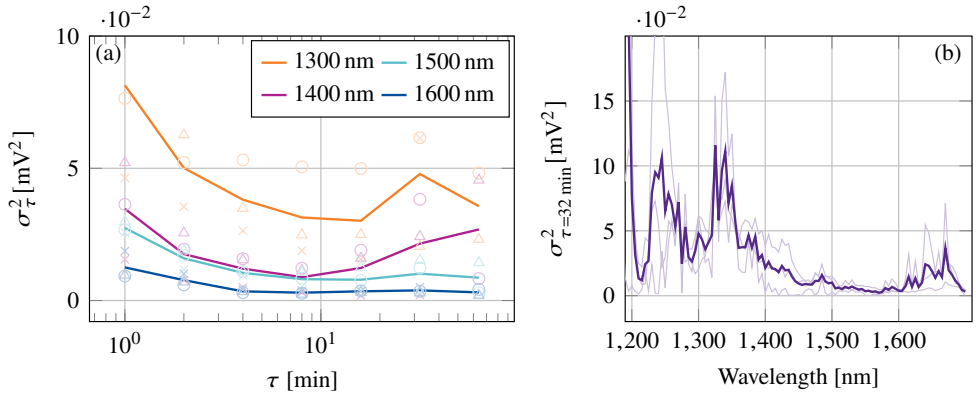

Fig. 9. (a) The mean Allan variance for a selection of wavelengths, together with the raw measurements. (b) The mean Allan variance for all the recorded wavelengths for $\tau = 32$ min, with the three raw traces in the background.

3.3. Case study: Glucose measurements

Discrete measurements

A prediction model was obtained by using cross-validation and a PLSR model with 3 latent variables. The result of the analysis of the discrete glucose measurements are shown in Figure 10(a). A root mean square error of cross validation (RMSECV) of 4.8 mM was obtained. The spectra after median filtering in the spectral domain (three points) and subtracting the previous PBS reference is shown in Figure 10(b). The obtained mean absolute relative difference (MARD) was 24.3 %. The glucose absorption has a similar shape to what was predicted in Figure 1(b), although the main absorption peak is somewhat blue-shifted (~ 1580 nm → 1610 nm). This discrepancy could be due to the temperature not being identical (20 °C vs. 37 °C in Figure 1(b)) or that assumptions of ideal conditions, such as imperfect split ratios, were not fulfilled for the experimental setup. The ripples across the spectrum are caused by features of the experimental setup and are not glucose features. The SNR of the system was determined to be 55.4 dB. The decrease in SNR compared to the short-term system is likely due to uncompensated drift and mechanical changes due to the sample procedure, but is an in-use bound for the system.

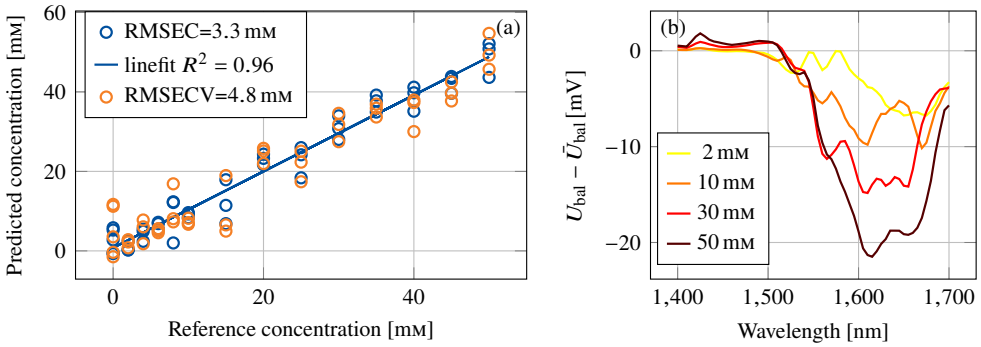

Fig. 10. (a) The prediction from a multivariate regression on the measurement series. (b) Examples of difference spectra with glucose concentrations that are used as the input to the model.

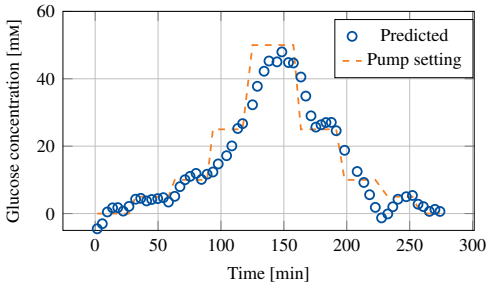

Fig. 11. Predicted glucose concentration with solution continuously pumped across the transmission cell to simulate the change in concentration in a body fluid.

Continuous measurements

To simulate a glucose measurement series in the human body, a pump was continuously pumping glucose solution to the sample arm of the transmission cell. The result of a prediction model built on the stabilized measurements (4 latent variables) is shown in Figure 11. There is a delay of approximately 10–15 min between setting the glucose concentration on the pump until the solution reaches the transmission cell. An oscillation was observed in the predicted response on several measurement series, which was attributed to imperfect mixing in the tubing and less accurate control with a large plunger and low flow-rates. The perceived signal stability was improved by taking the median across six scans. A three point moving mean was added to the measurement series to remove the oscillations caused by the pump plunger. The deviation from the pumped concentration around 225 min can be caused by the instability of the pumped concentration. Although this measurement series can not quantify the error due to pump and mixing instability, it shows that it is possible to obtain a prediction across a time series of several hours with liquid constantly flowing through the measurement system.

4. Discussion and conclusion

We have experimentally explored the use of a commercial SC laser source for fully fiber coupled broadband absorption spectroscopy sensing in the NIR range. Introducing a reference arm, balanced detector, and signal averaging, noise suppression of 2 orders of magnitude was achieved,

along with a SNR of 66 dB without the transmission cells and a long-term SNR of 55 dB including transmission cells and sample exchange. We present a thorough characterization of the system and can point to specific limitations and improvements for future use of SC sources in low-noise absorption spectroscopy measurement systems:

1. A balanced detector is required to reduce the noise levels, especially the effects of RIN noise and quantization error on the small signal.
2. The stability and reproduciblity of the fiber splitter are of high importance and could be improved further.
3. The wavelength range is limited to the SM operation of the fibers.
4. The transmission cell must be engineered with high precision and extremely stable components.

We use glucose sensing as a model system requiring very high accuracy, and we are able to obtain an accuracy approaching a benchtop free space beam spectrometer, shown in Figure 12.

Long-term instability

Although the short-term stability was shown to be acceptable for glucose sensing with averaging, the long-term stability limits the achievable accuracy. The balance was shown to be an important factor, but spectra were also not completely stable on the well-balanced wavelengths. Neither the temperature measured nor low bandwidth reference measurements from one of the arms (to detect larger changes in split ratio) could properly explain the changes, that were slightly different from measurement series to measurement series and looked like an oscillation across the spectrum. It was possible to partially correct for the drift by taking a blank reference spectrum within 15 min. The observed changes with time are likely due to a combination of change in temperature and strain as the experiment progressed and looked similar to previously reported spectral modal noise [18] for a system with few modes interfering. The use of a MM fiber to collect the light may be the cause of this. The ripples across the spectra seen in Figure 10(b) are not due to glucose, but rather noise likely caused by modal instability. In Figure 10(b), the advantage of scanning across several wavelengths is clear, it is easier to mitigate noise using a prediction model that takes into account the broad spectral features.

System variance and glucose measurements accuracy

With the development of the system, several series of glucose measurements have been obtained on different systems within our group. The root mean square error (RMSE) of these measurements is plotted against the standard deviation of the systems measured in Figure 12. As expected, there is a clear relationship between the noise level and the obtained glucose measurement error. Using an SC source without any reference arm gave a very low accuracy, and RMSE above 60 mM. A substantial improvement was obtained by implementing a reference arm. In the first iteration, measurements of the input pulse powers without passing through water as reference were conducted, and the correction was performed by dividing the output pulse power by the input pulse power [11]. In that setup, a relatively slow oscilloscope with 8 bit resolution was used. The system presented here gave a substantial performance improvement compared to that, with RMSE below 5 mM. To compare to the state-of-the-art NIR benchtop spectrometers, we also include the results of a measurement series on a Metrohm benchtop spectrometer with 1 mm cuvettes measured [39]. The error in repetability measurements using the benchtop spectrometer was calculated to 0.003 % based on measurements and noise levels [39, 40]. This is the level that a NIR system should reach in order to have acceptable measurement uncertainty for in vivo

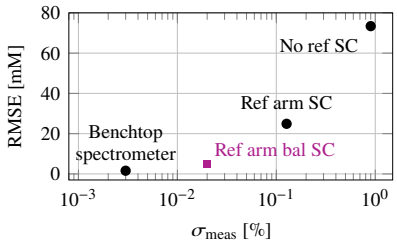

Fig. 12. Case study glucose monitoring: Plot of the RMSECV versus the measured standard deviation using different system configurations. The points correspond to: no reference arm for an SC source, a reference arm but unequal split between the arms (details in [11]) and two single detectors, the system presented here, and a benchtop spectrometer (details in [39]).

use. We obtained a SNR of 55 dB for the glucose measurements, which could not resolve 1 mM glucose changes which we estimated would need 70 dB.

The state of the art continuous glucose sensors are mostly electrochemical, one sensor on the market is based on optical readout [23]. The error is most often stated as MARD or points within a consensus error grid. For these sensors, the MARD is commonly around 11 % [41] but has also been reported up to 18 % [42]. With the experimentally obtained MARD of 24.3 % that was obtained in vitro in this study, small improvements are needed before it would be possible to make use of the system for continuous physiological glucose measurements.

Comparison to similar work

To the best of our knowledge, this is the first time that an SC source is used in a fully fiber-coupled absorption spectroscopy setup without the more common use of bulk optics [8, 9, 43–45]. In transitioning to a fully fiber-optic setup, issues arise with the stability that we have characterized and improved upon.

Ultra-high repetition rate absorption spectroscopy applied to gas sensing often labeled supercontinuum broadband absorption spectroscopy (SCLAS) use a dispersive fiber to temporally separate the wavelengths in a pulse [8–10, 44], which allows for rapid measurements as well as improved correction algorithms in post-processing. For narrow linewidth absorbers, a fit to the absorption trace can provide a reference signal and give a stable measurement without a reference arm setup. However, the temporally resolved pulse requires an extremely fast detector and ADC, which increases the cost of such a system. Furthermore, a dispersion compensation module might require several km of dispersion compensating fiber. These systems are not entirely comparable to ours. As Kaminski et al. note [44], the requirement for a broadly absorbing species and narrow absorbing lines also differ, and a balanced cell must be implemented to cope with the high RIN of SC sources for broadly absorbing species such as aqueous samples instead of using a correction algorithm.

Guo et al. [46] have proposed a similar system as the one presented, albeit using what appears to be bulk optics coupled transmission cells. They measured glucose concentrations down to 5 mg/dL (0.28 mM) with a tailored system centered around an SC source in the combination band, which has been favored alone or in combination with the first overtone band for glucose sensing [34, 35]. It is possible to use extended InGaAs sources to reach this wavelength region, but they also have higher noise floors, costs, and require cooling. Unfortunately, this aspect was not discussed in [46]. In comparison, our results were not as accurate (RMSECV 4.8 mM), although the short-term noise levels were comparable to ours and they report an SNR of 47 dB (compared to 55 dB here). The improvement in their results is likely due to the choice of wavelength region.

We aimed at using commercially available equipment and had a cost perspective in mind. Guo et al. [46] used a scanning monochromator that was relatively slow, giving a measurement time of 10 min. Using an AOTF in our setup is advantageous because it decreases the acquisition time so that a full scan can be performed within 4 min, including averaging. Their results along with the study presented here, point towards the applicability of SC sources in applications that require extremely low noise such as glucose sensing.

Outlook and possibilities

To achieve high stability for accurate measurements, every component must be optimized for the wavelength range: use of SM optical fibers, a stable beam splitter, as stable as possible source, and as accurate as possible balance between the detectors. As was outlined in the theory, a good balance with a CMRR of 30 dB can reduce the noise levels down to 3 % of the original values. It is difficult to achieve a perfect balance including transmission through the sample and reference absorption cells across a wide wavelength range. A balanced detector with a programmable wavelength dependent gain for the two detectors could be a solution to compensate the difference in split values and the differences in the reference and sample cells. The end stability can be further increased with a source with lower RIN. Recent advances in low-noise supercontinuum source development [5] show that the technology could be optimized beyond the instrument used here. With the cost perspective in mind, long pulsed SC lasers are advantageous (a low-noise ps source is 5-10 times the cost of our ns source [3]). The measurement speed can also be increased, as shown by applications of SC lasers applied to gas sensing (SCLAS), where the pulse is dispersed in time [10, 44] and not filtered so that the acquisition times can be on the order of one wavelength in our setup. The viability and cost of such an approach depends on the analyte requirements on wavelength resolution and wavelength range to select an appropriate dispersive element, detector, and ADC.

When laser RIN was suppressed, the dominant noise source contributing on a longer time scale was modal noise from the transmission cell and the MM collecting fibers. SM fibers have cores with diameter around 8 µm, which can be extended up to 25 µm for some photonic crystal SM fibers, which make them more difficult to couple into without using free space optics. Strategies using lensed fibers can increase the transmission somewhat [47]. For an even more stable system, replacing the splitter and interaction region by integrated optics could be a potential solution. SM fibers could be used to connect to the integrated optical platform, utilizing a stable splitter [48] and an exposed waveguide to perform evanescent field sensing [49].

Funding. Content in the funding section will be generated entirely from details submitted to Prism.

Acknowledgments. The Central Norway Regional Health Authority is acknowledged for the support to Silje S. Fuglerud, project number 46055510. The Research Council of Norway is acknowledged for supporting the Double Intraperitoneal Artificial Pancreas project, project number 248872, and the support of Jong W. Noh through Lab-on-a-chip Biophotonic Sensor Platform for diagnostics, project number 248869/O70. We thank Jana Jagerska for helpful tips on experimental aspects, detailed discussions, and research insights.

Disclosures. The authors declare no conflicts of interest.

Data Availability Statement. Data underlying the results presented in this paper are available in Ref. [50].

Supplemental document. See Supplement 1 for supporting content.

References

1. C. Pasquini, "Near infrared spectroscopy: A mature analytical technique with new perspectives – a review," Anal. Chimica Acta **1026**, 8–36 (2018).
2. K. B. Beć, J. Grabska, and C. W. Huck, "Principles and applications of miniaturized near-infrared (NIR) spectrometers," Chem. A Eur. J. **27**, 1514–1532 (2021).

3. M. Maria, I. B. Gonzalo, T. Feuchter, M. Denninger, P. M. Moselund, L. Leick, O. Bang, and A. Podoleanu, "Q-switch-pumped supercontinuum for ultra-high resolution optical coherence tomography," Opt. Lett. **42**, 4744–4747 (2017).
4. M. Jensen, I. B. Gonzalo, R. D. Engelsholm, M. Maria, N. M. Israelsen, A. Podoleanu, and O. Bang, "Noise of supercontinuum sources in spectral domain optical coherence tomography," JOSA B **36**, A154–A160 (2019).
5. S. Rao D. S., M. Jensen, L. Grüner-Nielsen, J. T. Olsen, P. Heiduschka, B. Kemper, J. Schnekenburger, M. Glud, M. Mogensen, N. M. Israelsen, and O. Bang, "Shot-noise limited, supercontinuum-based optical coherence tomography," Light. Sci Appl **10**, 133 (2021).
6. C. W. Freudiger, W. Yang, G. R. Holtom, N. Peyghambarian, X. S. Xie, and K. Q. Kieu, "Stimulated raman scattering microscopy with a robust fibre laser source," Nat. Photonics **8**, 153–159 (2014).
7. F. Crisafi, V. Kumar, T. Scopigno, M. Marangoni, G. Cerullo, and D. Polli, "In-line balanced detection stimulated raman scattering microscopy," Sci. Rep. **7**, 1–8 (2017).
8. S. Dupont, Z. Qu, S. Kiwanuka, L. Hooper, J. Knight, S. Keiding, and C. Kaminski, "Ultra-high repetition rate absorption spectroscopy with low noise supercontinuum radiation generated in an all-normal dispersion fibre," Laser Phys. Lett. **11**, 075601 (2014).
9. N. G. Blume and S. Wagner, "Broadband supercontinuum laser absorption spectrometer for multiparameter gas phase combustion diagnostics," Opt. Lett. **40**, 3141–3144 (2015).
10. J. Emmert, N. G. Blume, A. Dreizler, and S. Wagner, "Data analysis and uncertainty estimation in supercontinuum laser absorption spectroscopy," Sci. Rep. **8**, 1–16 (2018).
11. S. S. Fuglerud, K. Milenko, R. Ellingsen, A. Aksnes, and D. R. Hjelme, "Feasibility of supercontinuum sources for use in glucose sensing by absorption spectroscopy," in *Clinical and Preclinical Optical Diagnostics II,* (Optical Society of America, 2019), pp. 11073–13.
12. K. Seto, T. Tsukada, Y. Okuda, E. Tokunaga, and T. Kobayashi, "Development of a balanced detector with biased synchronous detection and application to near shot noise limited noise cancelling of supercontinuum pulse light," Revi Sci Instrum **85**, 023702 (2014).
13. K. Nose, Y. Ozeki, T. Kishi, K. Sumimura, N. Nishizawa, K. Fukui, Y. Kanematsu, and K. Itoh, "Sensitivity enhancement of fiber-laser-based stimulated raman scattering microscopy by collinear balanced detection technique," Opt. Express **20**, 13958–13965 (2012).
14. B. S. Kawasaki, K. O. Hill, and Y. Tremblay, "Modal-noise generation in biconical-taper couplers," Opt. Lett. **6**, 499–501 (1981).
15. P. J. Severin and W. H. Bardoel, "Bandwidth and modal noise effects in fused-head-end multimode fiber passive components," J. Light. Technol. **7**, 1932–1940 (1989).
16. S. Das, C. G. Englefield, and P. A. Goud, "Modal noise and distortion caused by a longitudinal gap between two multimode fibers," Appl. Opt. **23**, 1110–1115 (1984).
17. Grupp, F., "The nature of the fiber noise with the FOCES spectrograph - nature, modeling and a way to achieve S/N 400," A & A **412**, 897–902 (2003).
18. C.-H. Chen, R. O. Reynolds, and A. Kost, "Origin of spectral modal noise in fiber-coupled spectrographs," Appl. Opt. **45**, 519–527 (2006).
19. S. Delbeck, T. Vahlsing, S. Leonhardt, G. Steiner, and H. M. Heise, "Non-invasive monitoring of blood glucose using optical methods for skin spectroscopy—opportunities and recent advances," Anal. Bioanal. Chem. **411**, 63–77 (2019).
20. J. L. Smith, "The pursuit of noninvasive glucose: "Hunting the deceitful turkey", seventh edition," (2020). Available online: https://www.researchgate.net/publication/343695948_The_Pursuit_of_Noninvasive_Glucose_Hunting_the_Deceitful_Turkey_Seventh_Edition (accessed on August 2nd 2021).
21. M. K. Åm, K. Kölle, A. L. Fougner, I. Dirnena-Fusini, P. C. Bösch, R. Ellingsen, D. R. Hjelme, Øyvind Stavdahl, S. M. Carlsen, and S. C. Christiansen, "Effect of sensor location on continuous intraperitoneal glucose sensing in an animal model," PLoS ONE **13** (2018).
22. M. K. Åm, A. L. Fougner, R. Ellingsen, D. R. Hjelme, P. C. Bösch, Øyvind Stavdahl, S. M. Carlsen, and S. C. Christiansen, "Why intraperitoneal glucose sensing is sometimes surprisingly rapid and sometimes slow: A hypothesis," Med. Hypotheses **132**, 109318 (2019).
23. I. L. Jernelv, K. Milenko, S. S. Fuglerud, D. R. Hjelme, R. Ellingsen, and A. Aksnes, "A review of optical methods for continuous glucose monitoring," Appl. Spectrosc. Rev. **54**, 543–572 (2019).
24. B. E. Saleh and M. C. Teich, *Fundamentals of photonics; 2nd ed.* (Wiley, 2007).
25. E. Oliva, M. Rainer, A. Tozzi, N. Sanna, M. Iuzzolino, and A. Brucalassi, "Experimental characterization of modal noise in multimode fibers for astronomical spectrometers," A & A **632**, A21 (2019).
26. K. Sayood, "Scalar quantization," in *Introduction to Data Compression (Fourth Edition),* K. Sayood, ed. (Morgan Kaufmann, 2012), The Morgan Kaufmann Series in Multimedia Information and Systems, pp. 251 – 294, 4th ed.
27. A. K. Amerov, J. Chen, and M. A. Arnold, "Molar absorptivities of glucose and other biological molecules in aqueous solutions over the first overtone and combination regions of the near-infrared spectrum," Appl. Spectrosc. **58**, 1195–1204 (2004).
28. P. C. D. Hobbs, "Ultrasensitive laser measurements without tears," Appl. Opt. **36**, 903–920 (1997).
29. Thorlabs, *Balanced Amplified Photodetectors, PDB440A, PDB440A-AC, PDB440C, PDB440C-AC, PDB450A,*

PDB450A-AC, PDB450C, PDB450C-AC, Operation Manual.
30. R. Pallás-Areny and J. G. Webster, "Common mode rejection ratio in differential amplifiers," IEEE Trans Instrum Meas **40**, 669–676 (1991).
31. M. Goodarzi, S. Sharma, H. Ramon, and W. Saeys, "Multivariate calibration of NIR spectroscopic sensors for continuous glucose monitoring," TrAC Trends Anal. Chem **67**, 147 – 158 (2015).
32. K. J. Jeon, I. D. Hwang, S. J. Hahn, and G. Yoon, "Comparison between transmittance and reflectance measurements in glucose determination using near infrared spectroscopy," J. Biomed. Opt. **11**, 014022 (2006).
33. W. Yang, N. Liao, H. Cheng, Y. Li, X. Bai, and C. Deng, "Determination of NIR informative wavebands for transmission non-invasive blood glucose measurement using a fourier transform spectrometer," AIP Adv. **8**, 035216 (2018).
34. J. Chen, M. A. Arnold, and G. W. Small, "Comparison of combination and first overtone spectral regions for near-infrared calibration models for glucose and other biomolecules in aqueous solutions," Anal. Chem. **76**, 5405–5413 (2004). PMID: 15362899.
35. M. Goodarzi and W. Saeys, "Selection of the most informative near infrared spectroscopy wavebands for continuous glucose monitoring in human serum," Talanta **146**, 155–165 (2016).
36. K. Linga, G. Olsen, V. Ban, A. Joshi, and W. Kosonocky, "Dark current analysis and characterization of $In_xGa_{1-x}As/InAs_yP_{1-y}$ graded photodiodes with $x > 0.53$ for response to longer wavelengths ($> 1.7\,\mu m$)," J. Light. Technol. **10**, 1050–1055 (1992).
37. C. Besikci, "Extended short wavelength infrared FPA technology: status and trends," in *Quantum Sensing and Nano Electronics and Photonics XV,* vol. 10540 M. Razeghi, G. J. Brown, J. S. Lewis, and G. Leo, eds., International Society for Optics and Photonics (SPIE, 2018), pp. 110 – 125.
38. R. M. Kurtz and T. C. Forrester, "Optimizing reception bandwidth of a pulsed signal," in *Laser Radar Technology and Applications XXV,* vol. 11410 M. D. Turner and G. W. Kamerman, eds., International Society for Optics and Photonics (SPIE, 2020), pp. 77 – 95.
39. S. S. Fuglerud, R. Ellingsen, A. Aksnes, and D. R. Hjelme, "Investigation of the effect of clinically relevant interferents on glucose monitoring using near-infrared spectroscopy," J. Biophotonics **14**, e202000450 (2021).
40. Metrohm, *NIRS XDS RapidContent Analyzer, Manual*.
41. G. Freckmann, M. Link, U. Kamecke, C. Haug, B. Baumgartner, and R. Weitgasser, "Performance and usability of three systems for continuous glucose monitoring in direct comparison," J. Diabetes Sci. Technol **13**, 890–898 (2019).
42. R. Z. Jafri, C. A. Balliro, F. El-Khatib, M. M. Maheno, M. A. Hillard, A. O'Donovan, R. Selagamsetty, H. Zheng, E. R. Damiano, and S. J. Russell, "A three-way accuracy comparison of the Dexcom G5, Abbott Freestyle Libre Pro, and Senseonics Eversense continuous glucose monitoring devices in a home-use study of subjects with type 1 diabetes," Diabetes Technol. & Ther. **22**, 846–852 (2020).
43. R. Watt, C. Kaminski, and J. Hult, "Generation of supercontinuum radiation in conventional single-mode fibre and its application to broadband absorption spectroscopy," Appl. Phys. B **90**, 47–53 (2008).
44. C. Kaminski, R. Watt, A. Elder, J. Frank, and J. Hult, "Supercontinuum radiation for applications in chemical sensing and microscopy," Appl. Phys. B **92**, 367–378 (2008).
45. M. P. Halloran, J. Choi, T. Lee, and J. Yoo, "High-speed supercontinuum laser absorption spectroscopy of light hydrocarbons in elevated pressures and temperatures," Meas. Sci Technol **32**, 095502 (2021).
46. K. Guo, R. A. Martinez, M. Freeman, H. S. Gurm, and M. N. Islam, "High SNR glucose monitoring using a SWIR super-continuum light source," in *Conference on Lasers and Electro-Optics,* (Optical Society of America, 2016), p. AM4J.5.
47. S. S. Fuglerud, K. B. Milenko, R. Ellingsen, A. Aksnes, and D. R. Hjelme, "Glucose sensing by absorption spectroscopy using lensed optical fibers," Appl. Opt. **58**, 2456–2462 (2019).
48. D. González-Andrade, C. Lafforgue, E. Durán-Valdeiglesias, X. Le Roux, M. Berciano, E. Cassan, D. Marris-Morini, A. V. Velasco, P. Cheben, L. Vivien, and C. Alonso-Ramos, "Polarization-and wavelength-agnostic nanophotonic beam splitter," Sci. Rep. **9**, 1–9 (2019).
49. E. Ryckeboer, R. Bockstaele, M. Vanslembrouck, and R. Baets, "Glucose sensing by waveguide-based absorption spectroscopy on a silicon chip," Biomed. Opt. Express **5**, 1636–1648 (2014).
50. S. S. Fuglerud, "Performance improvement in a supercontinuum fiber-coupled system for near infrared absorption spectroscopy," https://doi.org/10.18710/IZ63JH (2021).